PHYSICAL REVIEW B **92**, 201302(R) (2015)

Influence of interface coupling on the electronic properties of the Au/MoS_2 junction

Matt Cook, Robert Palandech, Keith Doore, Zhipeng Ye, Gaihua Ye, Rui He, and Andrew J. Stollenwerk*
University of Northern Iowa, Department of Physics, 215 Begeman Hall, Cedar Falls, Iowa 50614-0150, USA
(Received 24 July 2015; published 6 November 2015)

Thin films of Au ranging from 7–24 nm were grown on MoS_2 at room temperature using thermal evaporation and studied using scanning tunneling microscopy and ballistic electron emission spectroscopy. Topographic images show the surface morphology of Au transitions from terraced triangles to a mix of terraced hexagonal and irregular-shaped structures as film thickness exceeded 16 nm. Raman spectra reveal the presence of tensile strain in the MoS_2 with thicker Au films and is likely the driving force behind this transition. All samples exhibit a Schottky barrier significantly lower than that predicted by the Schottky-Mott model due to Fermi-level pinning at the interface. The pinning mechanism is thought to be caused, in part, by the presence of gap states induced by a weakening of the interlayer Mo-S bonding in the presence of the Au film. Although relatively consistent in thinner films, the Schottky barrier increases concurrently with structural changes on the surface. At the same time, transmission through the interface begins to drop at an increased exponential rate with film thickness. These observations are consistent with a widening separation between the Au and MoS_2 that would reduce the number of gap states and cause transmission through the interface to be more characteristic of quantum tunneling. An increased separation such as this could result from changes in equilibrium conditions at the interface with increasing strain.

DOI: 10.1103/PhysRevB.92.201302 PACS number(s): 73.30.+y, 68.35.−p

Research surrounding layered materials has experienced a surge in activity since graphene was recently isolated [1,2]. By exploring these two-dimensional crystals, we increase our understanding of fundamental physics and can discover material systems with practical applications. Of particular interest are materials with band gaps given the broad range of applications in devices such as field-effect transistors (FETs) and, in the case of direct band-gap materials, optoelectronic devices. One such material with promise is MoS_2, which is known to have an indirect band gap of 1.29 eV in bulk that quickly transforms to a direct band gap of 1.9 eV when reduced to a monolayer [3]. Further, MoS_2-based FETs have already demonstrated high electron mobilities and on/off ratios [4,5]. Successful integration of MoS_2 into an electronic device requires metallic contacts chosen to form either an ohmic or rectifying interface, depending on the application.

The Schottky-Mott equation predicts the Schottky barrier height at rectifying interfaces based on the work function of the metal and the electron affinity of the semiconductor, $\phi_{SB} = \phi_m - \chi_{sc}$, but is typically incorrect to varying degrees due to Fermi-level pinning. Decades of study has shown that Fermi-level pinning in Si typically varies by about 0.2 eV regardless of the metal work function, doping concentrations, or interface impurities so that the Schottky barrier height is largely independent of material specifics. The mechanisms that shape the electronic structure of metal/MoS_2 contacts have remained more elusive due to seemingly contradictory results. For example, although Au/MoS_2 is reported to exhibit rectifying properties, both n-type and p-type characteristics have been observed in seemingly similar structures [6–11]. This is further complicated by several observations of ohmic interfaces [4,11]. For the most part, techniques used to characterize these interfaces have been limited to global measurements such as standard IV curves, making it difficult to reconcile these results. One notable exception is the use of light emission induced by scanning tunneling microscopy (STM) to probe the local electrical characteristics at the interface of Au islands on MoS_2 [9–11]. However, such nanojunctions are known to exhibit properties that can differ significantly from those of continuous films. Currently, there is a need for a more detailed investigation of the interface between continuous Au films on MoS_2 at a local scale.

One technique used to study the electronic properties of metal/semiconductor systems is ballistic electron emission microscopy (BEEM) [12,13]. The STM can be readily modified to accommodate BEEM measurements with nanometer-scale resolution. In the standard BEEM experiment, a bias V_t is applied so that electrons tunnel from the STM tip into a grounded thin-metal film, forming a Schottky contact with a semiconductor. Typically, the majority of electrons entering the metal enter the grounded contact and are measured as the STM current I_t. Those electrons that traverse the metal contribute to the BEEM current I_B, only with sufficient energy to surmount the Schottky barrier and available matching states in the conduction band. Currently, few studies have employed BEEM to study layered materials in any form. In this Rapid Communication, BEEM was used to characterize the electronic structure and transport properties across the Au/MoS_2 interface as a function of Au thickness and electron energy. No significant change was found with energy, but several unexpected thickness dependencies were observed that appear to correlate with surface morphology.

Samples were fabricated from commercially available MoS_2 substrates similar to those used in several recent studies [4,7,14]. A clean surface was exposed through mechanical exfoliation immediately before being introduced into the load lock of a home-built thermal deposition chamber with base pressure of 9×10^{-9} mbar. Au films were deposited onto the MoS_2 substrate at room temperature using a circular shadow mask with a 1.5 mm diameter at rate of approximately 0.1 Å/s monitored *in situ* using a quartz microbalance

*andrew.stollenwerk@uni.edu

previously calibrated against an atomic force microscope. Chamber pressure was kept below 5×10^{-8} mbar during film growth. Raman spectra of finished samples were taken at room temperature using a Horiba Labram HR Raman microscope system. A laser with 532 nm wavelength and a 100× objective lens with NA of 0.9 were used. The laser power was kept below 1 mW and was the same for all spectra taken. The instrument resolution was 0.5 cm^{-1} using a 1800 groove/mm grating.

A modified variable-temperature (100–600 K) UHV STM system (Omicron) was utilized to perform both BEEM and STM measurements. Samples were mechanically mounted to a BEEM sample holder *ex situ* using a conductive silver paste which also served as an ohmic backside contact as confirmed by standard I-V measurements. Electrical contact to the Au film was achieved by fixing a BeCu wire prior to being introduced into the STM/BEEM chamber with base pressure of 3×10^{-9} mbar. The STM sample stage was cooled using liquid nitrogen for all measurements to 110 K as measured by a Si diode in contact with the imaging stage. Tips were electrochemically etched from 0.25 mm W wire using a 5 M potassium hydroxide solution and a 5 V_{rms} bias. Ballistic electron emission spectroscopy was performed in a systematic grid fashion at a minimum of 900 locations over an area of approximately 1×1 μm. Typically, this measurement was repeated at several randomly chosen locations on the circular metal films. Individual spectra were averaged together in order to reduce the effects of surface roughness and electrical noise in the collector current.

Examples of topographic images from 7- and 12-nm-thick Au films are shown in Figs. 1(a) and 1(b), respectively. These surfaces are typical of those found on 7, 12, and 16 nm Au films and consist largely of terraced triangular structures with orientations reflecting the sixfold symmetry of the substrate. The triangular-shaped structures result from the initial stages of growth where three-dimensional triangular islands first nucleate and grow with a (111) orientation before eventually forming a continuous coverage as more Au is deposited [11,15–17]. The interface is known to be atomically smooth and only weakly bonded [15,17–19] such that it is possible to drag entire Au islands across the MoS_2 surface using an STM tip [20]. Thicker films exhibit a combination of hexagonal- and irregular-shaped structures such as those seen on the surface of the 20 nm film in Fig. 1(c). When the Au film is 24 nm thick, the surface is almost entirely composed of hexagonal structures, as seen in Fig 1(d).

The Raman spectra in Fig. 1(e) compares the vibrational modes associated with MoS_2 acquired from a bare surface to areas covered with 7 nm and 24 nm Au films. These data indicate that the A_{1g} out-of-plane vibration mode from MoS_2 does not shift after the deposition of Au, suggesting that the interlayer interaction in the MoS_2 substrate is not sensitive to the Au deposition. Similarly, there is no prominent shift of the in-plane E^1_{2g} mode of MoS_2 with the addition of a 7 nm Au film. However, the in-plane Raman mode displays a redshift of approximately 0.5 cm^{-1} after the deposition of 24 nm Au, better seen in the inset of Fig. 1(e). The softening of this in-plane phonon is consistent with a tensile strain on the order of about 0.3 % [21]. Given the lattice mismatch between the Au and MoS_2, it is possible that the strain in the thicker films occurs as the bulk properties of Au begin to dominate

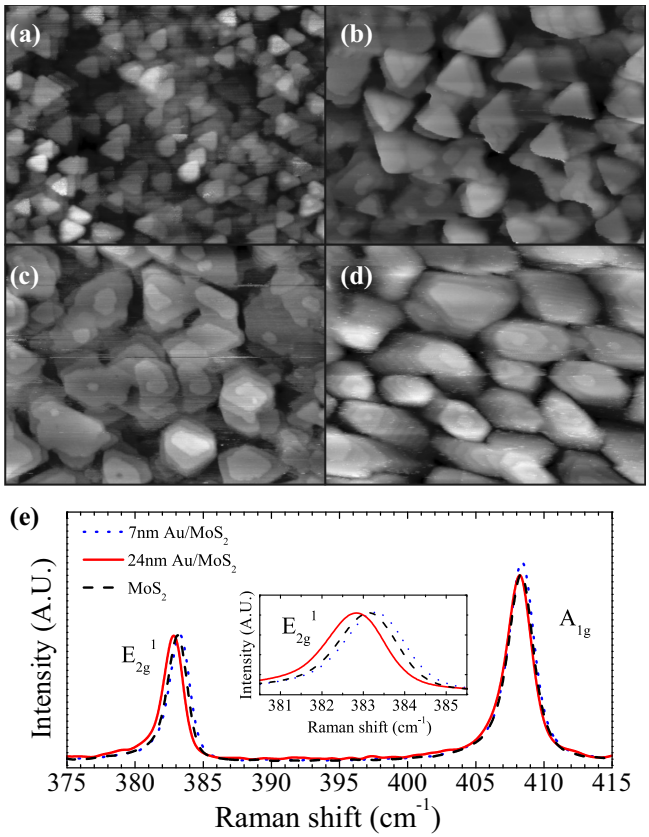

FIG. 1. (Color online) Topographic STM images of Au grown on MoS_2 with thicknesses of (a) 7, (b) 12, (c) 20, and (d) 24 nm. The dimension of each image is 80 × 60 nm. (e) Raman spectra acquired on bare MoS_2 and MoS_2 covered with 7 and 24 nm Au.

over interface contributions. The introduction of strain with increasing film thickness would account for the change in surface morphology.

Spectroscopy from samples fabricated under the same conditions and even from the same substrate with equal Au thickness was found to randomly display characteristics associated with both *n*-type and *p*-type MoS_2, with an overwhelming preference for *n*-type behavior. The evidence of both *n*-type and *p*-type characteristics was presented in previous studies and is believed to be the result of local variations in stoichiometry [7]. In those locations exhibiting *n*-type behavior, hot electrons were injected into the Au film to obtain BEEM spectra. The square root of the average transmission (I_B/I_t) for each thickness is presented in Fig. 2(a). Schottky barrier heights were extracted from these data using fits to the Bell-Kaiser (BK) model [12] and plotted as a function of Au thickness in Fig. 2(b). The Schottky barrier has a relatively consistent value of about 0.49 ± 0.02 eV from 7 to 16 nm before gradually increasing with thickness to 0.62 ± 0.02 eV at 24 nm.

These barrier heights are all significantly lower than that predicted by the Schottky-Mott equation, indicating that some form of Fermi-level pinning occurs at the interface. A number of different mechanisms have been proposed to account for Fermi-level pinning at metal/semiconductor interfaces, including chemical reactions [22,23], defects [23,24], and

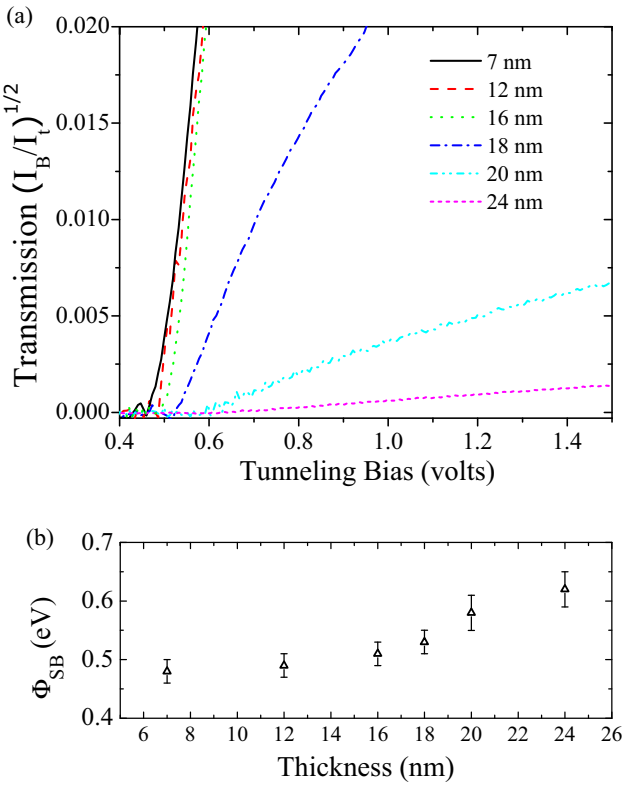

FIG. 2. (Color online) (a) Averaged BEEM spectra acquired from Au/MoS_2 samples with Au films ranging in thickness from 7 to 24 nm. (b) Corresponding Schottky barrier height as a function of Au thickness.

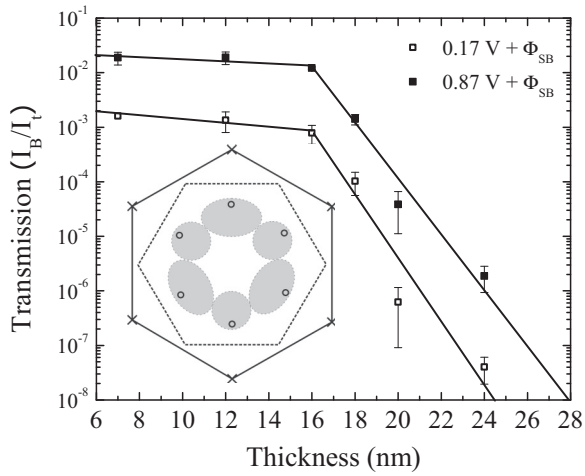

FIG. 3. Transmission through the Au/MoS_2 interface as a function of Au thickness at tunneling biases of 0.17 and 0.87 V above the Schottky height. Inset: Projected Au(111) Brillouin zone (dashed lines) onto the MoS_2(0001) Brillouin zone. Shaded regions represent the reciprocal space electron-beam size in Au as calculated in Ref. [37]. The projected MoS_2 conduction-band minima at K (x) and Λ (o) are superimposed.

metal-induced interfacial gap states [25]. The first seems unlikely in the Au/MoS_2 system as x-ray photoelectron spectroscopy (XPS) has ruled out reactions at the interface [7,26]. It is more probable that pinning would result from interfacial defects, as scanning tunneling spectroscopy shows the Fermi level at the surface of MoS_2 fluctuates on the nanometer scale by nearly 1 eV due to local variations in stoichiometry [7]. This is also consistent with the observation of n-type and p-type characteristics on the same MoS_2 substrate. A recent density functional theory (DFT) study of various metals on MoS_2 suggests that Fermi-level pinning can result from a significant charge redistribution at the interface that affects the work function of the metal [27]. Additionally, gap states form as intralayer Mo-S bonds weaken in the presence of metals. Both of these mechanisms depend greatly on the physical separation at the interface calculated to be 0.29 nm for Au(111) under equilibrium conditions [18,27]. Calculations show that enlarging this separation by 0.6 Å results in a roughly 130 meV increase in the Schottky barrier [27], similar to what is observed in Fig. 2(b). Given weak binding at the interface, it is possible the increasing Schottky barrier with film thickness is the result of a widening gap between the Au and MoS_2 as tensile strain changes the equilibrium spacing.

To account for a variable Schottky height, transmission values are compared relative to tunneling bias above the Schottky barrier. The thickness dependence of transmission is shown in the semi-log plot in Fig. 3 at tunneling biases of 0.17 and 0.87 V above the Schottky barrier. A clear change in transmission occurs at 16 nm as the signal begins to decrease at a greater rate. The two sets of lines through each of these data sets are fits to an exponential decay, $I_B/I_t \propto e^{[-d/\lambda(\epsilon)]}$, using thickness ranges of 7–16 nm and 16–24 nm. Here, d is Au thickness and λ is the effective electron attenuation length due to thickness-dependent scattering. The tunneling bias dependence of the attenuation length is plotted in Fig. 4 for thickness ranges of 7–16 nm [Fig. 4(a)] and 16–24 nm [Fig. 4(b)].

The actual attenuation length in a material does not vary with thickness without a change in dominant scattering mechanism or modification of the physical structure. The effective attenuation length as measured using BEEM is subject to additional variability. For example, several studies involving Au/Si(001) and Au/Si(111) have reported shorter attenuation lengths in Au films with thickness less than 10 nm due to a disproportional increase in the transmission of electrons that have undergone multiple reflections [28–30]. This is not observed here and likely due to a difference in scattering properties at the interface. The Au/Si interface tends to be highly disordered [31–36], resulting in a nearly isotropic electron distribution at the interface. Under these conditions, a significant number of incident electrons will lack matching states and not be initially transmitted into the Si. If the Au is thin enough, these electrons can make a second pass into the Si after backscattering into the Au and reflecting off the vacuum interface. These contributions quickly decrease with increasing Au thickness. When grown on MoS_2 at room temperature, Au forms highly oriented (111) islands with atomically smooth interfaces [17]. The inset in Fig. 3 shows the two-dimensional projection of the Au(111) Brillouin zone (BZ) onto the MoS_2(0001) BZ. From this image, it is clear that at energies just above the Schottky barrier, the electron current distribution in Au(111) [37] overlaps well with the MoS_2 conduction-band minimum at the Λ points, suggesting

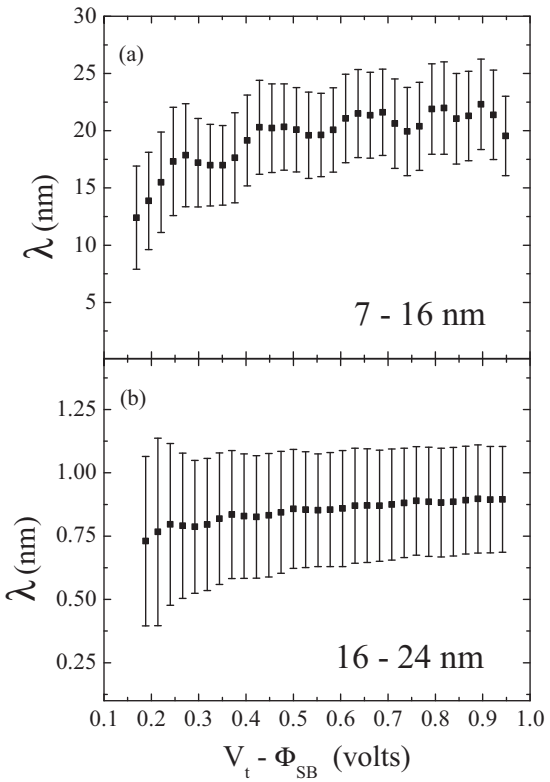

FIG. 4. Effective attenuation lengths measured in Au/MoS_2 for Au thickness ranging from (a) 7–16 nm and (b) 16–24 nm as a function of tunneling bias above the Schottky barrier.

comparatively little interfacial scattering and consequently less current contributions from multiple-reflected electrons.

Like the data in Fig. 3, attenuation lengths measured in Pd/Si are shorter in thicker Pd films [38]. This behavior was attributed to a transition in the dominant scattering mechanism from inelastic to elastic. However, such a transition has not been previously observed in Au/Si [28,30]. We also note that the attenuation lengths in Fig. 4(b) are more than an order of magnitude shorter than those found in lower-quality Au films grown on Si [39] and several times shorter than those measured in Fe films with significant C contamination [40]. For these reasons, we conclude that our observations are not the result of any change within the Au film. It is also unlikely that the changing surface morphology is directly responsible for a decrease in transmission spanning four orders of magnitude. As seen in the inset of Fig. 3, the interface band structure of $MoS_2(0001)$ does not have zone-centered conduction-band minima and will backscatter electrons with zero transverse momentum. Although the increase in atomically smooth regions on the surface of thicker Au films would suggest a more forward-focused current, the Au(111) band structure quickly redirects current away from the zone center [37]. Instead, we turn our attention to scattering at the Au/MoS_2 interface. Recent calculations predict a narrow tunneling barrier at the Au/MoS_2 interface [18,19] that would act to hinder transmission. If our previous conclusion is correct, we would expect transmission to decrease at a greater exponential rate as the Au/MoS_2 spacing steadily increases, consistent with the sudden drop in transmission at roughly 16 nm seen in Fig. 3.

In summary, several changes are observed in the Au/MoS_2 system as Au exceeds a critical thickness of approximately 16 nm. Structurally, the surface of the Au transitions from one of terraced triangles to a mix of terraced hexagonal- and irregular-shaped structures. A shift in the out-of-plane vibration mode of MoS_2 in the Raman spectra suggests greater tensile strain in samples with thicker Au films and is likely the mechanism responsible for the change in surface morphology. As these mechanical changes take place, the Schottky barrier increases by more than one-tenth of an eV. Recent DFT calculations suggest that Fermi-level pinning at the Au/MoS_2 interface is dependent on the proximity of these two materials. Increased separation between the Au and MoS_2 would weaken the pinning mechanisms and account for the greater Schottky height. This would also widen the thin tunneling barrier at the interface and account for the sudden drop in transmission as the Au thickness exceeds 16 nm. An increase in the spacing at the interface could result from changing equilibrium conditions with the introduction of strain in thicker Au films. Ultimately, these results are consistent with theory and provide insight into factors that affect the electronic properties of metal/MoS_2 interfaces.

This work was supported in part by the National Science Foundation (Grant No. DMR-1410496). A.J.S. was supported by a pre-tenure summer fellowship through the University of Northern Iowa. R.H. acknowledges partial support from the American Chemical Society Petroleum Research Fund (Grant No. 53401-UNI10). The authors wish to thank T. E. Kidd for useful discussions.

[1] K. S. Novoselov, A. K. Geim, S. V. Morozov, D. Jiang, M. I. Katsnelson, I. V. Grigorieva, S. V. Dubonos, and A. A. Firsov, Nature (London) **438**, 197 (2005).

[2] Y. Zhang, Y.-W. Tan, H. L. Stormer, and P. Kim, Nature (London) **438**, 201 (2005).

[3] K. F. Mak, C. Lee, J. Hone, J. Shan, and T. F. Heinz, Phys. Rev. Lett. **105**, 136805 (2010).

[4] B. Radisavljevic, A. Radenovic, J. Brivio, V. Giacometti, and A. Kis, Nat. Nanotechnol. **6**, 147 (2011).

[5] S. Kim, A. Konar, W.-S. Hwang, J. H. Lee, J. Lee, J. Yang, C. Jung, H. Kim, H. Kim, J.-B. Yoo, J.-Y. Choi, Y. W. Jin, S. Y. Lee, D. Jena, W. Choi, and K. Kim, Nat. Commun. **3**, 1011 (2012).

[6] W. Mönch, Appl. Phys. Lett. **72**, 1899 (1998).

[7] S. McDonnell, R. Addou, C. Buie, R. M. Wallace, and C. L. Hinkle, ACS Nano **8**, 2880 (2014).

[8] N. Kaushik, A. Nipane, F. Basheer, S. Dubey, S. Grover, M. M. Deshmukh, and S. Lodha, Appl. Phys. Lett. **105**, 113505 (2014).

[9] C. Maurel, F. Ajustron, R. Péchou, G. Seine, and R. Coratger, Surf. Sci. **600**, 442 (2006).
[10] C. Maurel, R. Coratger, F. Ajustron, J. Beauvillain, and P. Gerard, J. Appl. Phys. **94**, 1979 (2003).
[11] A. Carladous, R. Coratger, F. Ajustron, G. Seine, R. Péchou, and J. Beauvillain, Phys. Rev. B **66**, 045401 (2002).
[12] W. J. Kaiser and L. D. Bell, Phys. Rev. Lett. **60**, 1406 (1988).
[13] L. D. Bell and W. J. Kaiser, Phys. Rev. Lett. **61**, 2368 (1988).
[14] H. Liu, A. T. Neal, and P. D. Ye, ACS Nano **6**, 8563 (2012).
[15] J. Deng, C. Troadec, H. K. Hui, and C. Joachim, J. Vac. Sci. Technol. B **28**, 484 (2010).
[16] T. P. Darby and C. M. Wayman, Phys. Status Solidi A **25**, 585 (1974).
[17] S. Nagashima and I. Otsuka, J. Crystallog. Growth **146**, 266 (1995).
[18] I. Popov, G. Seifert, and D. Tománek, Phys. Rev. Lett. **108**, 156802 (2012).
[19] J. Kang, W. Liu, D. Sarkar, D. Jena, and K. Banerjee, Phys. Rev. X **4**, 031005 (2014).
[20] J. Yang, J. Deng, N. Chandrasekhar, and C. Joachim, J. Vac. Sci. Technol. B **25**, 1694 (2007).
[21] C. Rice, R. J. Young, R. Zan, U. Bangert, D. Wolverson, T. Georgiou, R. Jalil, and K. S. Novoselov, Phys. Rev. B **87**, 081307 (2013).
[22] L. J. Brillson, Phys. Rev. Lett. **40**, 260 (1978).
[23] R. T. Tung, Phys. Rev. Lett. **52**, 461 (1984).
[24] W. Spicer, T. Kendelewicz, N. Newman, K. Chin, and I. Lindau, Surf. Sci. **168**, 240 (1986).
[25] V. Heine, Phys. Rev. **138**, A1689 (1965).
[26] J. R. Lince, D. J. Carré, and P. D. Fleischauer, Phys. Rev. B **36**, 1647 (1987).
[27] C. Gong, L. Colombo, R. M. Wallace, and K. Cho, Nano Lett. **14**, 1714 (2014).
[28] L. D. Bell, Phys. Rev. Lett. **77**, 3893 (1996).
[29] M. W. Eckes, B. E. Friend, and A. J. Stollenwerk, J. Appl. Phys. **115**, 163710 (2014).
[30] M. K. Weilmeier, W. H. Rippard, and R. A. Buhrman, Phys. Rev. B **59**, R2521(R) (1999).
[31] E. Landree, D. Grozea, C. Collazo-Davila, and L. D. Marks, Phys. Rev. B **55**, 7910 (1997).
[32] L. Braicovich, C. M. Garner, P. R. Skeath, C. Y. Su, P. W. Chye, I. Lindau, and W. E. Spicer, Phys. Rev. B **20**, 5131 (1979).
[33] Z. Ma and L. H. Allen, Phys. Rev. B **48**, 15484 (1993).
[34] M. Iwami, T. Terada, H. Tochihara, M. Kubota, and Y. Murata, Surf. Sci. **194**, 115 (1988).
[35] K. Hricovini, J. Bonnet, B. Carrière, J. Deville, M. Hanbücken, and G. L. Lay, Surf. Sci. **211-212**, 630 (1989).
[36] C. Chen and L. Chen, Appl. Surf. Sci. **92**, 507 (1996).
[37] F. J. Garcia-Vidal, P. L. de Andres, and F. Flores, Phys. Rev. Lett. **76**, 807 (1996).
[38] R. Ludeke and A. Bauer, Phys. Rev. Lett. **71**, 1760 (1993).
[39] A. J. Stollenwerk, E. J. Spadafora, J. J. Garramone, R. J. Matyi, R. L. Moore, and V. P. LaBella, Phys. Rev. B **77**, 033416 (2008).
[40] A. J. Stollenwerk, M. R. Krause, D. H. Idell, R. Moore, and V. P. LaBella, Phys. Rev. B **74**, 155328 (2006).